# Temporal Integration of Olfactory Perceptual Evidence in Human Orbitofrontal Cortex

Nicholas E. Bowman,[1,*] Konrad P. Kording,[2] and Jay A. Gottfried[1,*]

[1]Department of Neurology, Northwestern University Feinberg School of Medicine, Chicago, IL 60611, USA

[2]Rehabilitation Institute of Chicago, Northwestern University, Chicago, IL 60611, USA

*Correspondence: nickbowman80@gmail.com (N.E.B.), j-gottfried@northwestern.edu (J.A.G.)

http://dx.doi.org/10.1016/j.neuron.2012.06.035

## SUMMARY

Given a noisy sensory world, the nervous system integrates perceptual evidence over time to optimize decision-making. Neurophysiological accumulation of sensory information is well-documented in the animal visual system, but how such mechanisms are instantiated in the human brain remains poorly understood. Here we combined psychophysical techniques, drift-diffusion modeling, and functional magnetic resonance imaging (fMRI) to establish that odor evidence integration in the human olfactory system enhances discrimination on a two-alternative forced-choice task. Model-based measures of fMRI brain activity highlighted a ramp-like increase in orbitofrontal cortex (OFC) that peaked at the time of decision, conforming to predictions derived from an integrator model. Combined behavioral and fMRI data further suggest that decision bounds are not fixed but collapse over time, facilitating choice behavior in the presence of low-quality evidence. These data highlight a key role for the orbitofrontal cortex in resolving sensory uncertainty and provide substantiation for accumulator models of human perceptual decision-making.

## INTRODUCTION

Perceptual decisions are routinely formed in the wake of imperfect sensory information. Behavioral performance improves, especially for noisy or weak sensory inputs, when animals take more time to sample the stimulus. For example, in the olfactory domain, a hunting dog may require multiple sniffs to decide whether a fast-moving rabbit has darted left or right under a hedgerow; a human may take several sniffs to decide whether a carton of milk on the verge of spoiling is a wise breakfast option. The implication is that the nervous system accumulates sensory information over time for efficient perceptual decision-making.

Neuroscientific support for the integration of noisy perceptual evidence is principally based on single-unit studies in nonhuman animals (Gold and Shadlen, 2007; Newsome et al., 1989; Platt, 2002; Romo and Salinas, 2001; Schall and Thompson, 1999). In a widely studied visual perceptual paradigm (Cook and Maunsell, 2002; Hanes and Schall, 1996; Newsome et al., 1989; Platt and Glimcher, 1999), responses in the lateral intraparietal area (LIP) show a ramp-like increase during a dot-motion discrimination task, such that animals make a decision when neuronal activity surpasses a bound (Roitman and Shadlen, 2002; Shadlen and Newsome, 2001). Such findings have helped inform and constrain models of perceptual decision-making.

Human imaging studies have begun using simple two-choice tasks to explore the neural substrates of visual perceptual decision-making (Heekeren et al., 2004; Huettel et al., 2005; Ivanoff et al., 2008; Noppeney et al., 2010; Ploran et al., 2007; Tosoni et al., 2008). However, the direct integration of perceptual evidence over time and its modulation by the degree of sensory noise are poorly understood. Resolving temporal integration using functional magnetic resonance imaging (fMRI) is difficult because humans tend to solve perceptual tasks much faster than the minimum data-acquisition rate of functional MRI scanners—too few data points are obtained per trial to allow the characterization of signal integration during the decision process. Traditional wisdom thus holds that fMRI is too slow to capture sensory integration (Noppeney et al., 2010; Philiastides and Sajda, 2007).

Here we took advantage of the fact that human olfactory perception evolves at a slow timescale, particularly for mixtures of odorants (Laing and Francis, 1989). This natural prolongation of response times implies that the olfactory system is ideally suited to characterize perceptual evidence integration with imaging techniques. In this study, we used fMRI to measure brain activity while subjects participated in a two-choice olfactory categorization task. Varying the relative proportion of components in a two-odorant mixture (Abraham et al., 2004; Boyle et al., 2009; Kepecs et al., 2008; Khan et al., 2008; Rinberg et al., 2006; Uchida and Mainen, 2003; Wesson et al., 2008) allowed us to manipulate odor mixture difficulty and to titrate the speed and accuracy of decision-making. With a combination of model-based fMRI approaches (O'Doherty et al., 2007), olfactory psychophysics, and deconvolution techniques (Glover, 1999; Zelano et al., 2009), we first established behaviorally that human subjects integrate odor information over time, particularly for difficult decisions, and then found that the profile of odor-evoked fMRI activity in medial orbitofrontal cortex (OFC) conforms to model simulations suggestive of evidence accumulation toward a decision bound.
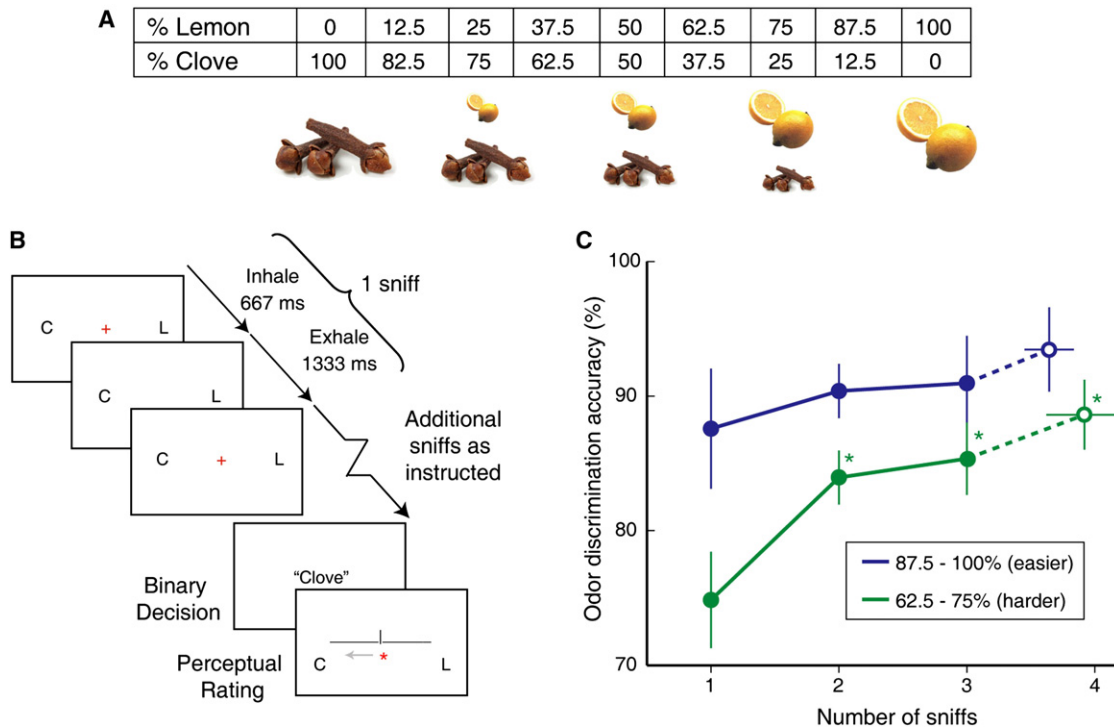
**Figure 1. Task Design and Behavioral Results from Experiment 1**

(A) The odorants eugenol (clove) and citral (lemon) were used to create nine different binary odorant mixtures ranging between 100% eugenol and 100% citral in 12.5% steps.

(B) Trial design depicting the two-alternative odor categorization task, with sniffs paced at 2 s intervals. Subjects inhaled when they saw a red crosshair on the screen (667 ms) and exhaled when it was not present (1333 ms). In separate blocks, subjects were instructed to make a fixed number of sniffs (one, two, or three), or an open number of sniffs. Visual cues C and L (clove and lemon, respectively) were used to remind subjects which response button corresponded to which choice.

(C) Psychophysical data from Experiment 1. Mean binary choice accuracy conditional on number of sniffs is plotted for fixed-sniff blocks (filled circles) and open sniff blocks (hollow circles). Performance accuracy (mean ± SEM) improved as subjects took more sniffs, particularly for more difficult odor mixtures (*p < 0.05, compared to one-sniff trials). Error bars: SEM.

## RESULTS

### Experiment 1: Odor Identification Accuracy Improves with More Sniffs

Although temporal integration in the visual system is well documented (Cook and Maunsell, 2002; Hanes and Schall, 1996; Platt and Glimcher, 1999), there is some controversy about whether such mechanisms take place in the olfactory system. In rodent models, a few studies indicate that rats require no more than one sample (sniff) to disambiguate odor mixtures (Kepecs et al., 2008; Uchida and Mainen, 2003; Wesson et al., 2008), while other work suggests that additional sniffs enhance perceptual performance (Abraham et al., 2004; Rinberg et al., 2006). Therefore, in Experiment 1, we set out to establish at the behavioral level whether the human olfactory system integrates information over time.

Healthy human subjects (n = 10) participated in a two-alternative forced-choice (2AFC) odor discrimination task, indicating which of two odor percepts was dominant in a set of odorant mixtures ranging between 100% eugenol ("clove") and 100% citral ("lemon"). Maximal mixture "difficulty" occurred with the

50% eugenol/50% citral mixture (Figure 1A). Stimulus mixtures were matched for perceived intensity, ensuring that subjects could not use this perceptual feature to guide their responses (see Supplemental Experimental Procedures available online). In separate blocks of trials, subjects were instructed to take one, two, or three sniffs, being cued to sniff every 2 s during stimulus presentation until the requisite number of sniffs had been taken. In a fourth block, subjects made additional sniffs until they reached a sufficient level of certainty regarding which of the two percepts dominated the mixture (Figure 1B).

The main hypothesis was that if integration exists, then the perceived quality of information should be greater with longer sampling times (more sniffs), resulting in higher performance accuracy. The psychophysical data, arranged into "less difficult" and "more difficult" mixture conditions, clearly show an improvement in accuracy as subjects took more sniffs (Figure 1C). The main effect of sniff number, tested across one-, two-, and three-sniff trials and collapsed across all mixture conditions, was significant ($\chi^2$ = 6.34, df = 2, p = 0.042; Friedman test for related samples), and this was particularly the case for the more difficult mixtures ($\chi^2$ = 8.21, df = 2, p = 0.017; Friedman
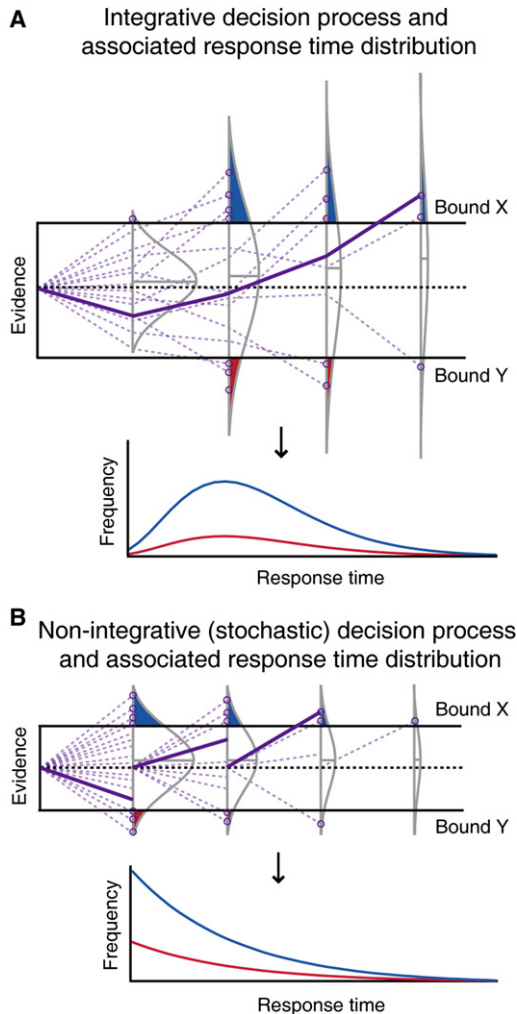
**Figure 2. Integrative and Nonintegrative Models of Decision-Making Generate Different Predictions about RT Probability Distributions**

(A) In an integrative decision process, successive samples of information, or "evidence," are accumulated over time, and a choice is made when that evidence crosses one of two decision bounds (X or Y, upper panel). This schematic shows integration of evidence (purple lines) for 16 sample trials, each terminating in a choice of X or Y (purple circles). Normal curves (gray lines) represent the distribution of evidence levels after each of four samples (simulated across many trials), where the shaded areas of the curves represent relative numbers of choices made at each sampling point for either X (blue) or Y (red). This decision process can be transformed into RT distributions for choices X (blue line) and Y (red line), which conform to gamma-distributed probability density functions (lower panel).

(B) In a nonintegrative (stochastic) decision process, each sample of information is independent of the previous samples, and a choice is made when a single sample has sufficient evidence to cross a bound (upper panel). The schematic also depicts 16 sample trials with four sampling points, but in this instance, if evidence does not surpass a threshold level, the decision process begins again at zero evidence for the next sample. The RT distributions arising from this nonintegrative process (lower panel) conform to exponentially decaying probability density functions. Specific sample trials (solid purple lines) in the upper panels of (A) and (B) depict differences in how evidence accrues over time in the two models.

test), but not for the less difficult mixtures ($\chi^2 = 0.64$, df = 2, p = 0.73). (For post hoc analyses and analyses of similar open-sniff profiles, see Supplemental Experimental Procedures.) Together these findings demonstrate performance gains with an increasing number of sniffs, especially for difficult mixtures, and are compatible with integrator models of perceptual decision-making in the human olfactory system.

**Experiment 2: Integration Accounts for RT Distributions in an Open-Sniff Task**

Given that the above results accord with olfactory temporal integration, in Experiment 2 we set out to elucidate this mechanism more extensively at the psychophysical and neuroimaging levels. To this end, fMRI brain activity was measured from an independent group of subjects (n = 11) participating in an olfactory 2AFC task. Odor stimuli, task design, and instructions were identical to the paradigm in Experiment 1, except that subjects made as many sniffs as needed ("open" sniffs) to decide which odorant dominated the mixture. Binary choices and response times (RTs) were both recorded. Critically, as opposed to Experiment 1, this open-sniff paradigm enabled us to define RT distribution functions that could be compared to those of integrative and nonintegrative (stochastic) models of perceptual decision-making (Figure 2) to provide support for either model.

We began by confirming that behavior in our olfactory task was consistent with profiles observed in other established perceptual decision-making paradigms (Gold and Shadlen, 2007). Psychometric data indicate that subjects successfully categorized eugenol-dominant mixtures as "clove" and citral-dominant mixtures as "lemon" (Figure 3A; for single-subject data, see Figure S1A). Subjects also rated odor mixtures with more citral as having a higher perceptual ratio of lemon relative to clove (Figure S1B). Decision accuracy was higher for the less difficult mixtures (at both ends of the mixture spectrum), exhibiting a sigmoidal relationship (R = 0.99 ± 0.001, group mean ± SEM; p < 0.0001) typical of 2AFC behavior (Luce, 1986; Ratcliff and McKoon, 2008; Wickelgren, 1977). Chronometric data similarly followed results in other sensory domains: subjects took more time when trying to categorize more difficult mixtures, and the RT profile across subjects showed a negative curvature of the best-fit parabola (p < 0.001; Wilcoxon sign-rank test) across the mixture continuum (Figure 3B; single-subject plots, Figure S1C).

We next used the behavioral data from Experiment 2 to simulate the RT distributions that would arise from a system accumulating information over time. Insofar as our findings accord with choice performance in other perceptual 2AFC studies, we modeled the psychophysical data (Figure 3) using a drift-diffusion model (DDM), which distills RT and accuracy data into two free parameters: the drift rate, which represents the mean rate of evidence accumulation; and the diffusion coefficient, which represents the variance around this accumulation. The DDM has been widely used to model behavior in tasks that rely on the temporal integration of information (Ditterich, 2006; Link and Heath, 1975; Mazurek et al., 2003; Ratcliff and McKoon, 2008). This model yields a gamma-like distribution of RTs. In parallel, a simulated RT distribution corresponding to a nonintegrative (stochastic) model was also implemented by removing
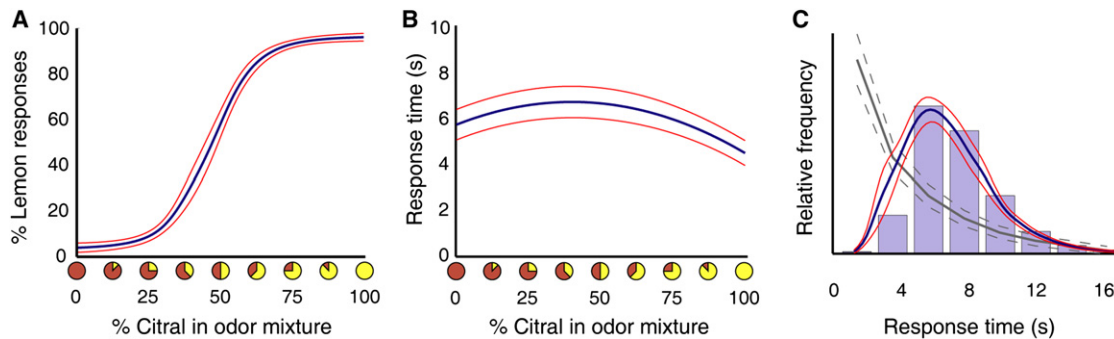
**Figure 3. Psychophysical Data from Experiment 2 Are Consistent with Drift-Diffusion Models of Integration**
(A) Group-averaged plots of performance accuracy demonstrate successful categorization of both odorants at each end of the odor mixture spectrum. Color wheels along the abscissa reflect relative proportions of eugenol-to-citral in each mixture (100% eugenol on the left; 100% citral on the right). The mean psychometric curve fit (blue line) was averaged across each subject's individually fitted sigmoidal function. Red curve, ± SEM.
(B) Group-averaged chronometric data demonstrate faster response times (RTs) for easier odor mixtures. Mean curve fit averaged across each subject's individually fitted parabolic function.
(C) A histogram plot of the RT data, binned into 2 s intervals, corresponds well to the gamma-like RT distribution arising from an integrative DDM (blue line), as opposed to the exponential RT distribution arising from a nonintegrative (stochastic) model (gray line).
See also Figure S1.

the integrator function from the DDM, yielding an exponentially decaying RT distribution. Comparison of these simulated RT distribution functions to the actual measured data (Figure 3) clearly demonstrates that the integrator model provides a better account of behavior than the nonintegrative model, and implies that the human olfactory system integrates sensory information over time in order to improve identification accuracy.

**Decision Bounds Collapse over Time**
An important follow-up question to the above analysis is how choice accuracy on this task relates to predictions from the DDM, and whether it can be used to demonstrate that the system benefits from increased sampling. Of note, if the decision-bound criterion is fixed over time (though see next paragraph), then in an open-response-time task, the accumulated information at the time of decision will be perceived to be of the same quality—upon reaching the decision bound—regardless of the time taken to reach that decision. It therefore follows that in an open-sniff task, accuracy for a given odor mixture will be the same for all observed RTs. That being said, for more difficult mixtures, overall accuracy may actually be lower, because the general quality of stimulus information is weaker, and subjects will have a greater probability of making the wrong choice. Plots of response accuracy conditional on number of sniffs (Figure 4A) demonstrate this mean reduction in decision accuracy for the hardest mixtures.

Interestingly, with regard to whether or not decision bounds are fixed, the fact that choice accuracy slightly declined for longer trials (compare three-sniff to five-sniff trials in Figure 4A) implies that subjects might be willing to accept a lower quality of evidence with the passage of time. This observation would be consistent with decision bounds that collapse over time, and such mechanisms have been hypothesized to occur in the visual system (Resulaj et al., 2009). Indeed a DDM simulation model with collapsing bounds closely reproduced behavioral accuracy on the open-sniff task from Experiment 2 (Figure 4B). Given these findings, we performed a new analysis to test

whether the fixed-bounds (standard) or collapsing-bounds DDM (cbDDM) provided a better fit to the behavioral data. A mean cumulative distribution function (CDF) of the RTs from the standard DDM was significantly different from the mean CDF of behavioral RTs ($p < 0.001$; Kolmogorov-Smirnov test), indicating that this model was a poor fit to the data (Figure 4C). However, the mean CDF of the cbDDM did not differ significantly from the mean CDF of behavioral RTs ($p = 0.1$) (Figure 4D), demonstrating that a DDM with collapsing bounds more accurately reflects the behavioral data than one with fixed bounds. Importantly, in terms of model selection, the cbDDM provided a statistically stronger fit than the standard DDM, even after adjusting for the number of free parameters using the Bayesian Information Criterion (BIC) (BIC: $7.61 \pm 1.06$; $p = 0.005$, t test; $p = 0.002$, Wilcoxon sign-rank test). Model simulations also revealed that the cbDDM provided a significantly better fit than a stochastic model with collapsing bounds, when tested against our data from 11 subjects ($p = 0.0044$, paired t test).

**Temporal Evidence Integration Is Unique to OFC**
With data across two experiments suggesting that humans integrate perceptual evidence over time, we next sought to characterize where this integration occurs in the brain. Although information might be expected to accumulate linearly over time, when the cbDDM is used to simulate the mean accumulated signal for trials of different lengths, it is evident that the time course of integration is nonlinear, increasing more rapidly closer to the time of decision (Figure 5A). Therefore, the behaviorally derived parameters from the cbDDM (including drift rate, diffusion coefficient, and collapse rate) were used, on a subject-by-subject basis, to model the expected temporal profile of information integration. These in turn were used to generate subject-specific fMRI regressors of interest in an event-related finite-impulse-response (FIR) model, enabling us to characterize within-trial temporal changes in the fMRI time series. Note that the absolute value of the integration profile
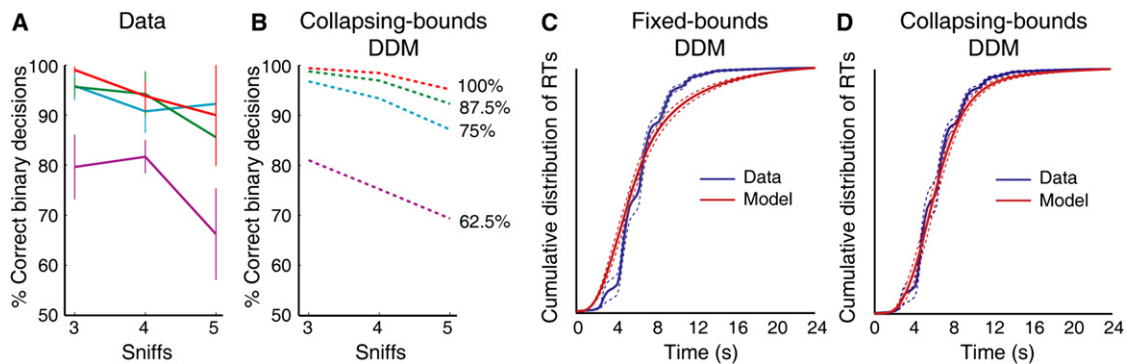
**Figure 4. Longer Trial Length Is Associated with Collapsing Decision Bounds**
(A) Behavioral accuracy conditional on sniff number is shown for four different mixture difficulty levels (100%: red; 87.5%: green; 75%: blue; 62.5%: purple), from the open-sniff paradigm in Experiment 2. Data are averaged across subjects and across mixture difficulty (e.g., 87.5% lemon trials and 87.5% clove trials represented as 87.5%).
(B) Model simulation of a collapsing-bounds DDM resembles the behavioral profiles in (A), demonstrating that, for the same mixture difficulty level, choice accuracy declines with longer trials.
(C) Cumulative distribution functions (CDFs) of the behavioral RTs (blue) significantly differed from the CDF of modeled RTs (red) based on a fixed-bounds DDM ($p < 0.001$; Kolmogorov-Smirnov test; two-sample). Mean, solid lines; ± SEM, dashed lines.
(D) In contrast, no significant difference was observed between the CDF of behavioral RTs and the CDF of modeled RTs from the collapsing-bounds DDM ($p > 0.05$).

was used to represent evidence toward *either* decision bound, and only trials of three, four, and five sniffs were included to ensure that sufficient numbers of trials across subjects were available for estimating the imaging data.

This approach revealed significant bilateral activity in centro-medial OFC ($p < 0.05$ small-volume corrected), near the anterior-medial portion of area 13l, (following the nomenclature of Ongür et al., 2003), and situated within the putative human olfactory OFC (Gottfried and Zald, 2005) (Figure 5B). To characterize the temporal profile of these activations as a function of trial length, deconvolution techniques (Glover, 1999; Zelano et al., 2009) were used to remove the low-pass effect of the fMRI hemodynamic response function on the mean time series in OFC. These plots show that activity increased at slower rates for longer trials, peaked at the time of decision, and had lower peaks for longer trials, suggestive of collapsing bounds (Figures 5C and 5D). Statistical analyses demonstrated a main effect of time (sniff number) in OFC (right mOFC, $p = 0.007$; left mOFC, $p = 0.021$; repeated-measures ANOVA) and a significant interaction between condition and time in right mOFC ($p = 0.032$) and at trend level in left mOFC ($p = 0.081$), demonstrating faster rates of increase for shorter trials. Additionally, a leave-one-subject-out cross-validation technique (Kriegeskorte et al., 2009) was used to obtain unbiased estimates of peak voxel activity in left and right OFC, and resulted in similar time series responses (Figure S2; Supplemental Experimental Procedures). These patterns conform closely to the temporal profiles predicted from the cbDDM model (cf. Figure 5A) and are consistent with olfactory information accumulation in human OFC.

Of note, the only other significant activations (at $p < 0.001$ uncorrected) from this fMRI model were in anterior OFC, anterior cingulate cortex (ACC), and cerebellum. In these instances, the fMRI time series plots from these regions (Figure 6) bear little resemblance to the integrating profiles in central OFC. Rather,

these data show that activity ramped up either at the same time, independent of trial length (e.g., anterior OFC and cerebellum), or at the same rate for all RTs (e.g., ACC). Indeed, while analyses of these time series demonstrate a main effect of time in each region (all $p < 0.003$), none of these regions exhibited a significant interaction of condition and time (all $p > 0.26$). Thus, these areas are likely involved in other aspects of odor information processing, whereas only the centromedial OFC appears to encode the accumulation of information over time in a manner consistent with model-derived integration profiles.

**Ongoing Sensory Report in Posterior Piriform Cortex**
In addition to the OFC, the piriform cortex has been implicated as a higher-order olfactory area involved in odor-quality coding, categorization, and discrimination in a variety of animal electrophysiological (Barnes et al., 2008; Schoenbaum and Eichenbaum, 1995; Tanabe et al., 1975) and human imaging (Gottfried et al., 2006; Howard et al., 2009; Small et al., 2008; Zelano et al., 2009) studies. Akin to the hierarchical electrophysiological dissociations between area MT and area LIP during visual perceptual decision-making, we hypothesized that posterior piriform cortex (pPC) generates an ongoing report of olfactory signals, whereas OFC integrates these signals. In order to determine the role that pPC plays in olfactory decision-making, we constructed anatomically defined regions of interest (ROIs) for both regions and then extracted and deconvolved the time series averaged across all voxels in each ROI for each subject.

In pPC the magnitude of activity peaked shortly after trial onset, and remained relatively sustained up until the time of decision (Figures 7A and 7B). Notably, trial duration had little effect on the time to peak: three-sniff, four-sniff, and five-sniff trials all reached their peaks by the second sniff. Analysis of the time series showed a main effect of time ($p < 0.001$), but no condition-by-time interaction ($p = 0.592$), demonstrating that
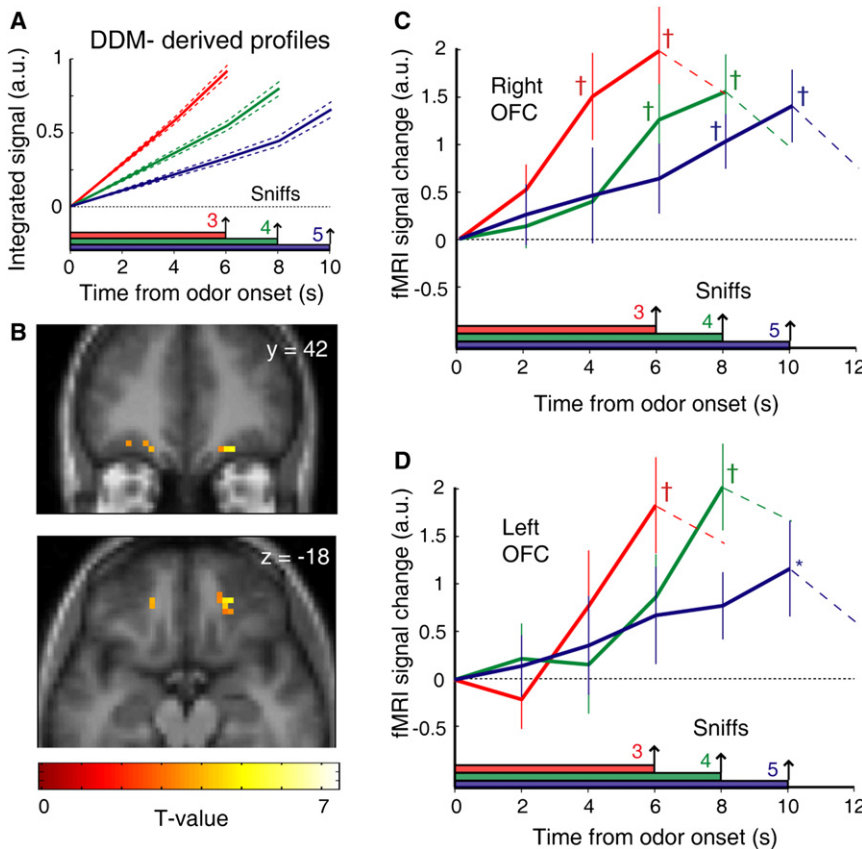
**Figure 5. Odor Evidence Integration in Medial OFC**

(A) Idealized time series profiles of evidence integration (mean, solid lines; SEM, dashed lines) for three-, four-, and five-sample (sniff) trials were generated from behaviorally derived parameters from each subject's collapsing-bounds DDM.

(B) Regression of the fMRI time series data against the integration profiles in (A) revealed significant activation in medial OFC ($p < 0.05$, small-volume corrected). Images overlaid on coronal (top) and axial (bottom) sections of the mean T1-weighted MRI scan (display threshold, $p < 0.005$).

(C and D) Group-averaged deconvolved fMRI time series (pooled across all significant voxels, $p < 0.005$) from right (C) and left (D) OFC demonstrate that orbitofrontal activity increases over time and peaks at the time of decision. All activations are normalized to odor onset. *$p < 0.05$; †, $p < 0.01$, differences from baseline. Error bars: SEM.

See also Figures S2, S3, and S5 and Table S1.

within-trial activity did not change at different rates, by condition. Thus, pPC appears to represent ongoing sensory information rather than integrate it for the purpose of perceptual decision-making. Activity from an anatomically defined ROI of anterior piriform cortex was also extracted, though its time series profile conformed neither to a representation of ongoing sensory information nor to the integration of this information (Figure S3).

By comparison, and in line with the fMRI time series data (Figure 5), condition-specific activity in OFC peaked only at the time of decision (Figures 7C and 7D). These time-course profiles also show that OFC activity gradually increased in magnitude up to the time of decision. As predicted by the cbDDM, for trials in which subjects took more time to make a decision, the response in OFC generally increased with a shallower slope and commenced later in the trial. There was both a main effect of time ($p = 0.024$) and a condition-by-time interaction ($p = 0.027$), demonstrating faster rates of increase for shorter trials. Similar OFC time series profiles were observed when the analysis was restricted either to mixtures of the same difficulty level (Figure S4) or to correct trials only (Figure S5), supporting the rationale behind combining trials of different stimulus difficulty and further confirming DDM predictions.

## DISCUSSION

The current results suggest that humans integrate olfactory perceptual evidence in order to enhance perceptual decision-making. These findings were supported across two independent psychophysical experiments. First, in a fixed-sniff paradigm, choice accuracy improved when subjects were given an opportunity to make more sniffs, especially for difficult odor mixtures (Figure 1C). This behavioral profile accords with temporal integration. Second, in an open-sniff paradigm, a drift-diffusion model of integration accounted for the resulting RT distributions significantly better than did a nonintegrative (stochastic) model (Figure 3D). This effect was particularly true when the simulation model incorporated decision bounds that collapsed over time (Figure 4).

The use of two complementary paradigms was necessary to establish that information accumulates in the human olfactory system. In the open-sniff paradigm, subjects only make a choice once a decision bound is reached, effectively clamping performance accuracy. This has the benefit of generating RT distributions that can be compared to model-derived RT distributions, such as the DDM, to provide evidence for or against integration. However, the open-sniff task is unable to demonstrate the type of choice-accuracy profiles that would be in keeping with integration. On the other hand, in the fixed-sniff paradigm, subjects make a response at a specified time, effectively disengaging their choices from a decision criterion. This has the potential benefit of eliciting behavioral accuracy profiles reflective of integration over time, although the resulting RT distributions (arising from imposed trial lengths) cannot be used to model integrative processing mechanisms. Together these two paradigms provide converging evidence that the human olfactory system, like other sensory systems, can integrate perceptual information.

Brain imaging data highlighted a corresponding fMRI signature of temporal integration in the OFC. Using a regionally unbiased approach, we found that odor-evoked activity in both right and left medial OFC conformed closely to integration profiles as predicted from the DDM (Figure 5). Specifically,
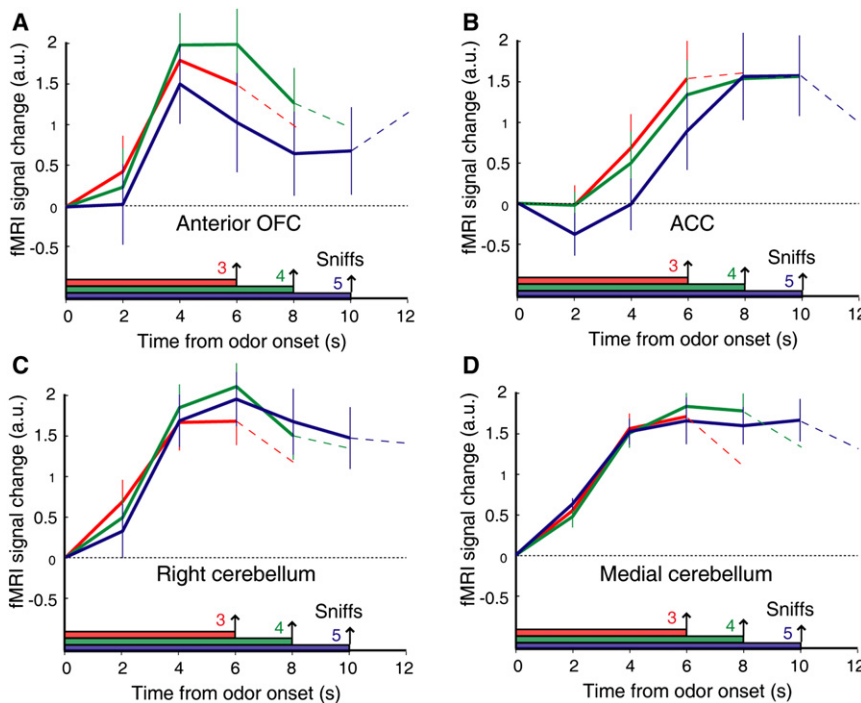
**Figure 6. Time Series Profiles of Increasing fMRI Activity in Other Brain Areas**

Correlations between the integration model and the FIR imaging data set identified several other regions with fMRI activity that increased over time (p < 0.001 uncorrected), including right anterior OFC (A), anterior cingulate cortex (B), right lateral cerebellum (C), and medial cerebellum (D). These time series, averaged across subjects (mean ± SEM, deconvolved) are not compatible with temporal integration, as predicted by the DDM. See also Table S1.

time series increased at slower rates for longer trials, peaked at the time of decision, and had lower peaks for longer trials. Of note, the anatomical locus of this response overlapped with the putative olfactory projection site in human OFC (Gottfried and Zald, 2005). Ramp-like activity patterns were also seen in cerebellum, ACC, and anterior OFC (Figure 6). However, none of these other regions exhibited a time-course profile in accordance with integration. These findings suggest that the medial OFC is selectively involved in the accumulation of olfactory perceptual evidence.

By comparison, fMRI activity in pPC reached a plateau soon after odor onset, and trial duration had negligible impact on the activation slopes (Figure 7). The distinct temporal response patterns in pPC and OFC suggest that olfactory system processing can be conceptualized as a two-stage mechanism in which odor evidence is represented in pPC and integrated in OFC. In elucidating a neurobiological mechanism that explicitly links sensory inputs with perceptual states and decision criteria, our findings help fill an important empirical gap in the human imaging literature on perceptual decision-making, and they bring models of human perceptual decision-making closely in line with animal single-unit recording studies. The functional dichotomy between pPC and OFC mirrors the respective roles played by areas MT and LIP in the encoding and integration of visual perceptual evidence in monkeys (Britten et al., 1992; Shadlen and Newsome, 2001), implying that common general mechanisms subserve perceptual decision-making across different sensory domains (Romo and Salinas, 2001).

Of course, there are important differences between our paradigm and more classical paradigms such as the visual motion discrimination task. Nevertheless, it is worth pointing out that conceptually, the dot-motion task and our task align in an impor-

tant way: at any given point of time, the central nervous system processes a noisy signal, whether this happens to be a snapshot of moving dots or a sniff of an odor mixture. Ideally, both moving dot patterns and odor quality information could be identified perfectly without any integration to speak of. For example, seeing a single pair of dots moving in the same direction should perfectly disambiguate the direction, yet intrinsic limitations originating in nervous system processing means that the brain has noisy access to this signal and therefore lacks the precision to arrive at a perceptual decision from just a brief glimpse (see, for example, Tassinari et al., 2006 and their Figure 3). That the signal fidelity of information (evidence) in the brain is not perfect is ultimately what gives rise to the need for integration. That being said, it is true that odor stimuli in general cannot be controlled nearly as precisely as can visual stimuli, nor are the stimulus adaptation characteristics as well defined in the olfactory system, thereby introducing less quantifiable stimulus noise. As mentioned above, a distinct advantage of using odors is that integration is relatively slow, which makes it ideal for visualizing with fMRI techniques.

Given that the DDM makes no specific assumptions about what is being integrated, it is important to ask what the mOFC signal represents. In a 2AFC task, this noisy sensory information gives rise to a probability that one or the other of the two perceptual categories dominates the stimulus. At each sampling step, it is this probability that is integrated with past-accumulated probabilities. Thus, in the framework of the DDM, signal accumulation in mOFC can be interpreted as the temporal integration of perceptual evidence toward a criterion bound, which when reached results in a decision. Interestingly, our data suggest that in OFC, these bounds collapse over time, underscoring a mechanism by which subjects are willing to accept an increasingly lower quality of sensory information to arrive at a decision. The idea of adaptable decision bounds, especially for error-prone trials, is supported by recent psychophysical data showing that new bound settings in the postdecision period may be used to either affirm or change a decision (Resulaj et al., 2009). Of course, the tendency for decision bounds to change will depend on task demands, with an emphasis on accuracy favoring bound constancy, and an emphasis on speed
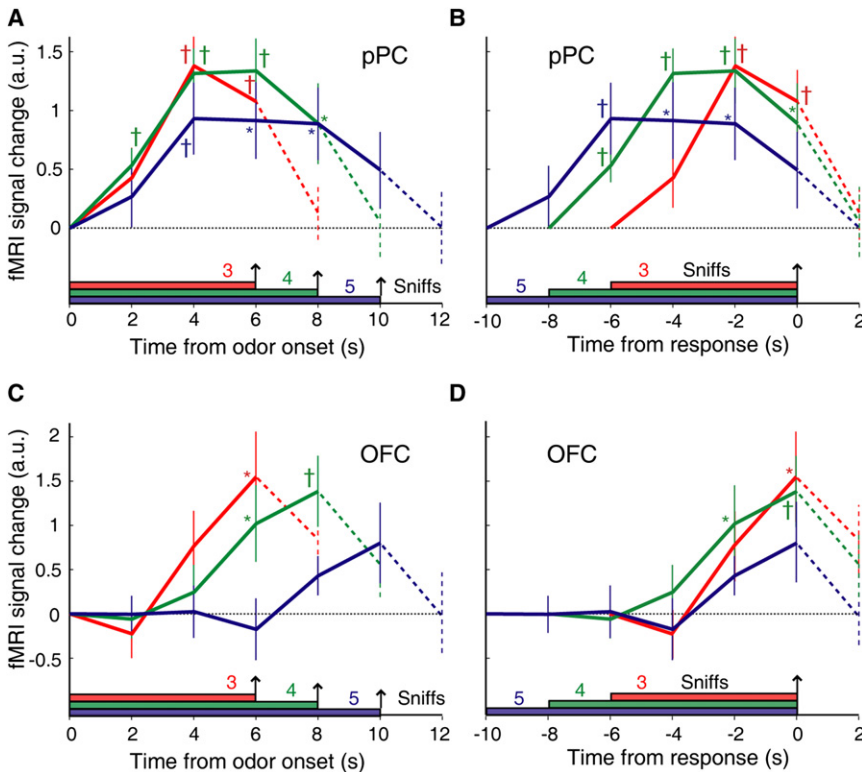
**Figure 7. Dissociable Representations of Odor Content and Odor Evidence Integration in pPC and OFC**

(A and B) An ROI analysis depicts the deconvolved time series of fMRI activity in posterior piriform cortex (pPC), aligned either to odor onset (A) or to response choice (B). These profiles demonstrate an early response take-off in pPC after odor onset and an early time to peak, with activity levels that remain sustained throughout the odor presentation period.

(C and D) In contrast, an ROI analysis of the deconvolved time series from olfactory OFC, also aligned to odor onset (C) or response time (D), shows ramp-like responses that peak at the time of decision, with shallower slopes for longer trials. Data at each time point for each sniff-length condition are averaged across subjects (mean ± SEM). All activations are normalized to odor onset. *p < 0.05; †, p < 0.01, differences from baseline. See also Figure S2.

2003, 2004; Schoenbaum et al., 1998; Schoenbaum and Eichenbaum, 1995; Tremblay and Schultz, 1999). This begs the question of whether a build-up of reward-related expectancy signals toward a decision could underlie our findings. However, subjects in our study were not rewarded for correct trials or given response feedback. Therefore, in the absence of explicit access to value or outcome information, the generation of a signal that encoded, and integrated, expected value over time would likely have been negligible.

Another alternative is that the within-trial increase in OFC activity represents a motor readiness signal, or an impetus to act, that increases over time as subjects converge on a decision. These "myoeconomic" arguments (Maunsell, 2004; Roesch and Olson, 2003, 2004) contend that the neuronal signatures of reward value in areas such as LIP or premotor frontal cortex more accurately represent motivational and motor preparatory responses engaged as an effect of reward anticipation. Again, because our subjects received no feedback or reward, there would not have been an opportunity for reward-based induction of motor readiness signals. Finally, whether the OFC signal reflects attention or arousal effects seems unlikely, because more difficult mixtures (more attentionally demanding) elicited the same magnitude of OFC activity as less difficult mixtures (see Supplemental Experimental Procedures).

The identification of olfactory evidence integration in OFC broadly accords with findings from a wide range of studies showing that integrative mechanisms are at the core of much of OFC function, including multisensory integration, associative (cue-outcome) learning, and experience-dependent perceptual plasticity. It also fits soundly with its suggested role in integrating information about unique outcomes in real time (Schoenbaum and Esber, 2010; Takahashi et al., 2009), particularly when experience alone is insufficient to formulate predictions about future events. Our new findings highlight the capacity of OFC

favoring bound collapse. These results highlight an intrinsic mechanism of speed-accuracy tradeoff, whereby the brain naturally relaxes decision criteria to avoid the loss of time associated with noisy evidence.

Investigations into the role that OFC plays in olfactory decision-making have been previously carried out in rodents. In a study by Kepecs and colleagues (Kepecs et al., 2008), single-unit recordings from OFC were made in awake, behaving rats engaged in a 2AFC discrimination task involving mixtures of two pure odorants. On each trial, rats sampled an odor mixture at a central port, and then responded by moving to either a left or right choice port, where it waited to receive a water reward for a correct response. Interestingly, during this postchoice, reward-anticipation period, orbitofrontal neurons fired more strongly on incorrect (versus correct) trials, as if OFC could gauge the quality of the decision even prior to receipt of reward, and neural responses in OFC mirrored a behavioral measure of decision confidence across mixture stimuli. These findings suggest that rodent OFC may encode confidence, whereby less confidence is associated with higher OFC activity. Indeed our OFC activity could possibly be interpreted as a confidence signal, insofar as increased evidence could theoretically be paralleled by an increase in confidence, but our study was not designed to address this specifically.

The idea that the signal in OFC reflects evidence integration toward a probability bound partially rests on ruling out other alternatives. For example, associative learning studies show that in the period leading up to reward delivery, OFC activity increases with reward magnitude, reward delay, and effort cost to earn reward (Kennerley et al., 2009; Roesch and Olson,

to maintain and integrate perceptual evidence online, enabling the olfactory system to extract meaningful perceptual signals from noisy inputs. As noted above, the fact that OFC stands at the transition between the olfactory system, limbic and paralimbic areas, and prefrontal cortex (Ongür et al., 2003) has important implications for understanding its unique role in higher-order control of odor-based behavior. The temporal instantiation of an odor percept in OFC could serve to orchestrate downstream effector systems, providing network coordination of autonomic, affective, and motor preparatory responses. In turn, centrifugal inputs from prefrontal executive areas to OFC could help regulate the decision boundary settings for integration. It remains to be determined whether orbitofrontal integration of perceptual evidence also plays a guiding role in nonolfactory paradigms of perceptual decision-making.

## EXPERIMENTAL PROCEDURES

### Subjects

Ten subjects (six women; age 23–27 years) participated in Experiment 1 and 12 subjects (six women aged 22–29 years) participated in Experiment 2. All were right-handed, without known neurological or olfactory deficits, and all provided informed consent to take part in the study, which was approved by the Northwestern University Institutional Review Board. One subject was excluded from Experiment 2 due to poor behavioral performance.

### Odorants and Odorant Delivery

Two odorants were selected that were relatively familiar, similar in pleasantness, and easily discriminable from each other: eugenol ("clove") and citral ("lemon"). All subjects were highly familiar with these odor categories, and were introduced to both stimuli prior to the main experiment so that they could easily associate names with the stimulus percepts. Odorants were diluted in diethylphthalate and matched for perceptual intensity (concentrations: citral, 50% v/v; eugenol, 33% v/v). Odorants were presented using an eight-channel MRI-compatible air-dilution olfactometer (airflow, 10 L/min), permitting precise delivery of two-odorant mixtures through a nasal mask. The ratio of the two odorants was modified by adjusting the relative proportion that each odorant channel contributed to the total airflow. Nine different odorant mixtures were used, morphing between 100% eugenol and 100% citral in 12.5% steps. Follow-up analyses ensured that odor intensities were the same across this mixture continuum and did not change during a trial or over the course of the experiment (Supplemental Experimental Procedures).

### Respiratory Monitoring

Subjects were instructed to keep their sniffs as similar as possible for each trial. Sniffs were measured with a spirometer attached to the nasal mask during Experiment 1, and with a pair of breathing belts affixed around the chest and abdomen (Howard et al., 2009) during Experiment 2. The output from these devices was processed using a PowerLab 8/30 data acquisition system (ADInstruments). Mean inspiratory volume in Experiment 2 did not significantly differ across odor mixtures ($F_{3.24,32.36}$ = 1.356; p = 0.273; repeated-measures ANOVA) or across sniff number ($F_{1.43,14.25}$ = 1.576; p = 0.238, three-, four-, and five-sniff trials).

### Experiment 1 Paradigm

Subjects performed a two-alternative forced-choice (2AFC) task, in which they indicated which of two olfactory perceptual qualities (lemon and clove) was dominant in an odorant mixture (citral and eugenol). Subjects completed four blocks of 36 trials in which each of the nine odor mixtures was presented four times in a random order (144 trials in total). At the beginning of each block, subjects were instructed to take either one, two, or three sniffs ("fixed-sniff" blocks), or as many sniffs as needed to make a reasonably confident decision regarding which one of the odorants dominated the stimulus mixture ("open-

sniff" blocks). The order in which these blocks were completed was counter-balanced across subjects. Each trial began with a visual countdown cue ("Prepare to sniff," "3," "2," "1") presented on a computer monitor. A sniff cue (red cross-hair) was then displayed for 667 ms, and recurred with a stimulus-onset asynchrony of 2 s to prompt additional sniffs, as necessary.

On the open-sniff trials, subjects made a binary choice with the left or right keyboard arrow once they had accumulated sufficient evidence that clove or lemon was dominating the mixture. Subjects were instructed to emphasize accuracy, ensuring that a decision would be made only when sufficient evidence had been accumulated to the criterion threshold. This was the primary instruction given to the subjects. They were incidentally reminded that upon reaching their decision, they should respond by button press as quickly as possible, so that recorded decision times closely reflected the time that they reached their decision.

At the end of each trial, subjects also made a perceptual rating on a visual analog scale ranging from pure clove to pure lemon, by moving a cursor from the midpoint of this continuum (representing equal proportions of the two odors). For the fixed-sniff trials, this estimate yielded binary choice measures according to which side of the midpoint the rating fell on. The next odor was presented 18 s after the end of the previous odor presentation, to minimize olfactory habituation. Binary decisions, analog ratings, and odor presentation times were recorded for each trial. Olfactory and visual stimuli presentations were controlled using Cogent2000 (http://www.vislab.ucl.ac.uk/cogent.php).

### Experiment 2 Paradigm

This was the same as Experiment 1, except that all trials were of the open-sniff type. Because this experiment took place in an MRI scanner, subjects responded using one of two button boxes held in either hand, one representing clove, the other lemon (hand side counter-balanced across runs). These buttons were also used to make the perceptual rating along a visual analog scale. Subjects were not told the outcomes of their decision, to prevent cognitive feedback or reward processing from confounding the neuroimaging findings. Sniffs were visually cued, as before, but were back-projected from a computer monitor onto a tilted mirror that was affixed to the MRI headbox in front of the subject's eyes. The letters "L" and "C" (lemon and clove) were presented on opposite sides of the screen to indicate which side represented which odor, and this was counterbalanced across subjects and sessions. Sniff rate was again set at two seconds in order to time-lock this to the data-acquisition rate of the MRI scanner (2,000 ms; see below). Subjects completed two runs of 36 trials on 2 consecutive days (four runs total) to minimize subject fatigue and odor habituation. Each of the nine mixtures was presented eight times each day (144 trials in total over 2 days), and trials were arranged in pseudorandom order such that every mixture preceded every other mixture one time to minimize effects of mixture sequence.

### Drift-Diffusion Modeling and Collapsing-Bounds Analysis

We determined the drift rate and the diffusion coefficient for each subject and condition by maximizing the probability of all experimentally observed responses, consisting of choices and RTs, given the drift and diffusion parameters. We assumed a symmetric drift-diffusion process (Resulaj et al., 2009), i.e., the same amount of information in favor of a hypothesis should be necessary for both lemon and clove choices. Moreover, given knowledge that drift rate, diffusion coefficient, and decision bound overspecify the model (whereby a doubling of these variables leads to identical behavior), we arbitrarily set the fixed bounds at ±1. The remaining two parameters of the model, drift and diffusion, define a joint probability distribution of choices and RTs that we calculated using the method of images. We then used a multidimensional unconstrained nonlinear minimization function ("fminsearch" in Matlab) to maximize the log probability of the actual RTs and choices. This led to a maximum-likelihood estimate of drift and diffusion, which were used to characterize behavior.

In order to test whether the response time data are better explained by collapsing bounds than by the standard fixed-bound DDM, an additional parameter of bound collapse rate was added to the DDM. The bounds were allowed to collapse linearly from 1 and −1, until they reached zero, at a rate determined by the model. Both models produced log-likelihood scores of

the model fit to the data, which were then compared to each other. Log-likelihood scores for a collapsing-bound stochastic model were also compared with those of the collapsing-bound DDM.

## Accuracy Modeling

The cbDDM randomly samples simulated "information" that has a normal distribution with a mean (signal) and variance (noise). It then integrates this information from trial to trial, and if the sum of the information crosses one of the decision bounds (arbitrarily chosen to start at ±1), a choice is recorded and the simulated trial ends. In this model, a value of 0 represents information with no evidence for either choice; if the integrator reached the positive bound, the trial was counted as a correct choice, and if it reached the negative bound, the trial was counted as an incorrect choice. The cbDDM-derived drift rate (signal), diffusion coefficient (noise), and bound collapse rate were used to simulate the decision process for each odor-mixture difficulty, for each subject, yielding accuracy for different RTs.

## Model-Based Integration Profiles

Integration profiles are nonlinear, due to a selection bias that skews which trials are more likely to cross the decision bound: trials in which integrated information has deviated farther from baseline are more likely to cross the decision bound as a result of the next sample; trials closer to baseline will be more likely to require more than one additional sample to reach the bound. Such bias results in an accumulation of information that on average is curvilinear, with a later take-off from zero for longer trials. Thus, to calculate temporal accumulation profiles (for regression against the fMRI data), we input drift rate (signal), diffusion (noise), and bound collapse rate into the DDM to generate time series of mean integrated evidence for each mixture group and each subject. We then generated mean time series for each condition (three-, four-, and five-sniffs) by weighting these mixture-based time series according to the relative number of trials for each sniff number (cf. Figure 5A).

## fMRI Data Acquisition

Functional imaging was performed using a Siemens Trio 3T MRI scanner to acquire gradient-echo T2*-weighted echoplanar images (EPIs) with blood-oxygen-level-dependent (BOLD) contrast, using a 12-channel head coil and an integrated parallel acquisition technique known as GRAPPA (GeneRalized Autocalibrating Partially Parallel Acquisition) to improve signal recovery in medial temporal and basal frontal regions.

Image acquisition was tilted 30° from the horizontal axis to reduce susceptibility artifact in olfactory areas. Four runs of ∼450 volumes each were collected in an interleaved ascending sequence (24 slices per volume). Imaging parameters were as follows: repetition time (TR), 2 s; echo time, 20 ms; slice thickness, 2 mm; gap, 1 mm; in-plane resolution, 1.72 × 1.72 mm; field of view, 220 × 206 mm; matrix size, 128 × 120 voxels. Whole-brain high-resolution T1-weighted anatomical scans (1 mm$^3$) were acquired after functional scanning, coregistered to the mean functional image, normalized, and averaged across subjects to aid in localization.

## fMRI Data Preprocessing

Data preprocessing and analysis were achieved using SPM5 (http://www.fil.ion.ucl.ac.uk/spm/). After the first six "dummy" volumes were discarded to permit T1 relaxation, images were spatially realigned to the first volume of the first session and slice-time adjusted. This was followed by spatial normalization to a standard EPI template, resulting in a functional voxel size of 3 mm$^3$, and smoothing with a 6-mm Gaussian kernel, aiding multisubject comparisons.

## fMRI Time Series Analysis

In Experiment 2, two different fMRI models were implemented to investigate the neural basis of olfactory evidence accumulation in the human brain. Three-, four-, and five-sniff conditions were selected for analysis because these contained sufficient numbers of trials across each subject for meaningful comparisons to be made. This method also ensured that data were not simply averaged across subjects with different response times, which would have introduced smoothing artifacts in the time-course data. It is important to reit-erate that the behavioral data (from which drift rates and integrator models were computed) were collected simultaneously during fMRI scanning.

### Finite Impulse Response Analysis

To investigate how region-specific fMRI time courses related to evidence integration, the preprocessed event-related fMRI data were analyzed using a finite impulse response (FIR) model, enabling us to model temporal integrative profiles. Selected conditions (three-, four-, and five-sniff trials) were specified using 14 time bins each of 2 s duration. Another condition including trials of all other sniff numbers was also included, as were six movement-related vectors, derived from spatial realignment. The data were high-pass filtered (cutoff, 128 s) to remove low-frequency drifts, and temporal autocorrelations were modeled using an AR(1) process.

Model estimation was carried out in two stages. First, subject-specific beta values (regression coefficients) were estimated for each time point and condition in a voxel-wise manner. From these first-level models, brain regions involved in evidence accumulation were identified by correlating fMRI activation time courses with model-based temporal profiles that estimated the amount of evidence integrating at each time point. These time series were convolved with a canonical hemodynamic response function (HRF) and then used to weight each of the 14 fMRI time points for each condition of interest (three, four, and five sniffs) with its corresponding integration value, yielding a contrast image, or statistical parametric map, of temporal integration.

In a second (random-effects) stage, the resulting subject-specific contrast images were entered into a one-sample t test, constituting a group-level statistical map, to identify brain regions potentially exhibiting temporal integration. All voxels with significant activation (p < 0.001 uncorrected) were considered for further analysis. For each region identified in this manner, time series plots were computed by averaging fMRI activity across all contiguous voxels significantly activated at p < 0.005 for each of the 14 time bins. Reported significant activations in OFC were corrected for multiple comparisons using small-volume correction, based on spheres of 10 mm radius centered on previously published coordinates (Gottfried and Zald, 2005).

### Region-of-Interest Analysis

This approach allowed us to investigate how temporal activity varied in a priori regions of interest, including aPC, pPC, and OFC, which have been previously implicated in fMRI studies of olfactory perceptual processing (Howard et al., 2009; Zelano et al., 2011). For this analysis, the realigned, slice-time corrected, and normalized, but unsmoothed, fMRI data were used to obtain raw time series on a voxel-by-voxel basis, thereby minimizing the influence of neighboring voxels. ROIs were structurally defined on the subject-averaged T1 structural scan using MRIcron (http://www.cabiatl.com/mricro/mricron/index.html). For the putative olfactory OFC, a sphere of 10 mm radius was drawn around the region's locus (Gottfried and Zald, 2005), delimited to gray matter using an MRIcron filter (threshold, 90–180; arbitrary units), yielding a bilateral ROI of volume 5,184 mm$^3$. Bilateral posterior and anterior piriform cortex ROIs were defined using prior landmarks (Howard et al., 2009; Zelano et al., 2011), yielding volumes of 2,106 and 1,485 mm$^3$, respectively.

ROI-specific time series were deconvolved using a regularized filter algorithm ("deconvreg" function in Matlab) to remove the low-pass filter properties of the HRF. These deconvolved time series were then divided into trials of different lengths. Mean time series were computed for all trials of the same length from a given ROI. Each time series was Z-transformed for each subject, using data from odor onset through the following 12 s, to include all relevant time points for all trial lengths. Following this step, the time series were normalized to activity at odor onset and linearly detrended. Mean activity was then plotted across subjects by aligning either to time of odor onset or to time of response (as in Figure 7).

## Statistical Analyses

For analysis of the behavioral data, nonparametric statistics were used, as follows: the Friedman test for more than two related samples, the Wilcoxon sign-rank test for paired comparison between two samples, and the Kolomogorov-Smirnov test for comparing actual and modeled RT distributions. All data are presented as the mean ± SEM. Statistical testing of the fMRI data and respiratory wave forms was implemented using one-tailed t tests (when

comparing activation to chance), two-tailed t tests (when comparing two conditions), or ANOVAs (when comparing more than two conditions). Results were considered significant at p < 0.05.

## REFERENCES

Abraham, N.M., Spors, H., Carleton, A., Margrie, T.W., Kuner, T., and Schaefer, A.T. (2004). Maintaining accuracy at the expense of speed: stimulus similarity defines odor discrimination time in mice. Neuron 44, 865–876.

Barnes, D.C., Hofacer, R.D., Zaman, A.R., Rennaker, R.L., and Wilson, D.A. (2008). Olfactory perceptual stability and discrimination. Nat. Neurosci. 11, 1378–1380.

Boyle, J.A., Djordjevic, J., Olsson, M.J., Lundström, J.N., and Jones-Gotman, M. (2009). The human brain distinguishes between single odorants and binary mixtures. Cereb. Cortex 19, 66–71.

Britten, K.H., Shadlen, M.N., Newsome, W.T., and Movshon, J.A. (1992). The analysis of visual motion: a comparison of neuronal and psychophysical performance. J. Neurosci. 12, 4745–4765.

Cook, E.P., and Maunsell, J.H. (2002). Dynamics of neuronal responses in macaque MT and VIP during motion detection. Nat. Neurosci. 5, 985–994.

Ditterich, J. (2006). Evidence for time-variant decision making. Eur. J. Neurosci. 24, 3628–3641.

Glover, G.H. (1999). Deconvolution of impulse response in event-related BOLD fMRI. Neuroimage 9, 416–429.

Gold, J.I., and Shadlen, M.N. (2007). The neural basis of decision making. Annu. Rev. Neurosci. 30, 535–574.

Gottfried, J.A., and Zald, D.H. (2005). On the scent of human olfactory orbitofrontal cortex: meta-analysis and comparison to non-human primates. Brain Res. Brain Res. Rev. 50, 287–304.

Gottfried, J.A., Winston, J.S., and Dolan, R.J. (2006). Dissociable codes of odor quality and odorant structure in human piriform cortex. Neuron 49, 467–479.

Hanes, D.P., and Schall, J.D. (1996). Neural control of voluntary movement initiation. Science 274, 427–430.

Heekeren, H.R., Marrett, S., Bandettini, P.A., and Ungerleider, L.G. (2004). A general mechanism for perceptual decision-making in the human brain. Nature 431, 859–862.

Howard, J.D., Plailly, J., Grueschow, M., Haynes, J.D., and Gottfried, J.A. (2009). Odor quality coding and categorization in human posterior piriform cortex. Nat. Neurosci. 12, 932–938.

Huettel, S.A., Song, A.W., and McCarthy, G. (2005). Decisions under uncertainty: probabilistic context influences activation of prefrontal and parietal cortices. J. Neurosci. 25, 3304–3311.

Ivanoff, J., Branning, P., and Marois, R. (2008). fMRI evidence for a dual process account of the speed-accuracy tradeoff in decision-making. PLoS ONE 3, e2635.

Kennerley, S.W., Dahmubed, A.F., Lara, A.H., and Wallis, J.D. (2009). Neurons in the frontal lobe encode the value of multiple decision variables. J. Cogn. Neurosci. 21, 1162–1178.

Kepecs, A., Uchida, N., Zariwala, H.A., and Mainen, Z.F. (2008). Neural correlates, computation and behavioural impact of decision confidence. Nature 455, 227–231.

Khan, A.G., Thattai, M., and Bhalla, U.S. (2008). Odor representations in the rat olfactory bulb change smoothly with morphing stimuli. Neuron 57, 571–585.

Kriegeskorte, N., Simmons, W.K., Bellgowan, P.S.F., and Baker, C.I. (2009). Circular analysis in systems neuroscience: the dangers of double dipping. Nat. Neurosci. 12, 535–540.

Laing, D.G., and Francis, G.W. (1989). The capacity of humans to identify odors in mixtures. Physiol. Behav. 46, 809–814.

Link, S., and Heath, R. (1975). A sequential theory of psychological discrimination. Psychometrika 40, 77–105.

Luce, R.D. (1986). Response Times: Their Role in Inferring Elementary Mental Organization (New York: Oxford University Press).

Maunsell, J.H. (2004). Neuronal representations of cognitive state: reward or attention? Trends Cogn. Sci. 8, 261–265.

Mazurek, M.E., Roitman, J.D., Ditterich, J., and Shadlen, M.N. (2003). A role for neural integrators in perceptual decision making. Cereb. Cortex 13, 1257–1269.

Newsome, W.T., Britten, K.H., and Movshon, J.A. (1989). Neuronal correlates of a perceptual decision. Nature 341, 52–54.

Noppeney, U., Ostwald, D., and Werner, S. (2010). Perceptual decisions formed by accumulation of audiovisual evidence in prefrontal cortex. J. Neurosci. 30, 7434–7446.

O'Doherty, J.P., Hampton, A., and Kim, H. (2007). Model-based fMRI and its application to reward learning and decision making. Ann. N Y Acad. Sci. 1104, 35–53.

Ongür, D., Ferry, A.T., and Price, J.L. (2003). Architectonic subdivision of the human orbital and medial prefrontal cortex. J. Comp. Neurol. 460, 425–449.

Philiastides, M.G., and Sajda, P. (2007). EEG-informed fMRI reveals spatiotemporal characteristics of perceptual decision making. J. Neurosci. 27, 13082–13091.

Platt, M.L. (2002). Neural correlates of decisions. Curr. Opin. Neurobiol. 12, 141–148.

Platt, M.L., and Glimcher, P.W. (1999). Neural correlates of decision variables in parietal cortex. Nature 400, 233–238.

Ploran, E.J., Nelson, S.M., Velanova, K., Donaldson, D.I., Petersen, S.E., and Wheeler, M.E. (2007). Evidence accumulation and the moment of recognition: dissociating perceptual recognition processes using fMRI. J. Neurosci. 27, 11912–11924.

Ratcliff, R., and McKoon, G. (2008). The diffusion decision model: theory and data for two-choice decision tasks. Neural Comput. 20, 873–922.

Resulaj, A., Kiani, R., Wolpert, D.M., and Shadlen, M.N. (2009). Changes of mind in decision-making. Nature 461, 263–266.

Rinberg, D., Koulakov, A., and Gelperin, A. (2006). Speed-accuracy tradeoff in olfaction. Neuron 51, 351–358.

Roesch, M.R., and Olson, C.R. (2003). Impact of expected reward on neuronal activity in prefrontal cortex, frontal and supplementary eye fields and premotor cortex. J. Neurophysiol. 90, 1766–1789.

Roesch, M.R., and Olson, C.R. (2004). Neuronal activity related to reward value and motivation in primate frontal cortex. Science 304, 307–310.

Roitman, J.D., and Shadlen, M.N. (2002). Response of neurons in the lateral intraparietal area during a combined visual discrimination reaction time task. J. Neurosci. *22*, 9475–9489.

Romo, R., and Salinas, E. (2001). Touch and go: decision-making mechanisms in somatosensation. Annu. Rev. Neurosci. *24*, 107–137.

Schall, J.D., and Thompson, K.G. (1999). Neural selection and control of visually guided eye movements. Annu. Rev. Neurosci. *22*, 241–259.

Schoenbaum, G., and Eichenbaum, H. (1995). Information coding in the rodent prefrontal cortex. I. Single-neuron activity in orbitofrontal cortex compared with that in pyriform cortex. J. Neurophysiol. *74*, 733–750.

Schoenbaum, G., and Esber, G.R. (2010). How do you (estimate you will) like them apples? Integration as a defining trait of orbitofrontal function. Curr. Opin. Neurobiol. *20*, 205–211.

Schoenbaum, G., Chiba, A.A., and Gallagher, M. (1998). Orbitofrontal cortex and basolateral amygdala encode expected outcomes during learning. Nat. Neurosci. *1*, 155–159.

Shadlen, M.N., and Newsome, W.T. (2001). Neural basis of a perceptual decision in the parietal cortex (area LIP) of the rhesus monkey. J. Neurophysiol. *86*, 1916–1936.

Small, D.M., Veldhuizen, M.G., Felsted, J., Mak, Y.E., and McGlone, F. (2008). Separable substrates for anticipatory and consummatory food chemosensation. Neuron *57*, 786–797.

Takahashi, Y.K., Roesch, M.R., Stalnaker, T.A., Haney, R.Z., Calu, D.J., Taylor, A.R., Burke, K.A., and Schoenbaum, G. (2009). The orbitofrontal cortex and ventral tegmental area are necessary for learning from unexpected outcomes. Neuron *62*, 269–280.

Tanabe, T., Iino, M., and Takagi, S.F. (1975). Discrimination of odors in olfactory bulb, pyriform-amygdaloid areas, and orbitofrontal cortex of the monkey. J. Neurophysiol. *38*, 1284–1296.

Tassinari, H., Hudson, T.E., and Landy, M.S. (2006). Combining priors and noisy visual cues in a rapid pointing task. J. Neurosci. *26*, 10154–10163.

Tosoni, A., Galati, G., Romani, G.L., and Corbetta, M. (2008). Sensory-motor mechanisms in human parietal cortex underlie arbitrary visual decisions. Nat. Neurosci. *11*, 1446–1453.

Tremblay, L., and Schultz, W. (1999). Relative reward preference in primate orbitofrontal cortex. Nature *398*, 704–708.

Uchida, N., and Mainen, Z.F. (2003). Speed and accuracy of olfactory discrimination in the rat. Nat. Neurosci. *6*, 1224–1229.

Wesson, D.W., Carey, R.M., Verhagen, J.V., and Wachowiak, M. (2008). Rapid encoding and perception of novel odors in the rat. PLoS Biol. *6*, e82.

Wickelgren, W.A. (1977). Speed-accuracy tradeoff and information processing dynamics. Acta Psychol. (Amst.) *41*, 67–85.

Zelano, C., Montag, J., Khan, R., and Sobel, N. (2009). A specialized odor memory buffer in primary olfactory cortex. PLoS ONE *4*, e4965.

Zelano, C., Mohanty, A., and Gottfried, J.A. (2011). Olfactory predictive codes and stimulus templates in piriform cortex. Neuron *72*, 178–187.